Excited States of Bridged [14]Annulenes

Laura Moroni, Cristina Gellini, and Pier Remigio Salvi*

Dipartimento di Chimica, Universitá di Firenze, via della Lastruccia 3, 50019 Sesto Fiorentino, Firenze, Italy

Emanuel Vogel

Institut für Organische Chemie, Universität Zu Köln, Greinstrasse 4, 50939 Köln, Germany

Received: June 11, 2004; In Final Form: July 23, 2004

Fluorescence and Raman spectra of two representative bridged [14]annulenes, i.e., 1,6:8,13-ethanediylidene[14]-annulene and 1,6:8,13-propanediylidene[14]annulene (**1** and **2** in Figure 1, respectively) have been measured. The fluorescence spectra show a resolved Franck−Condon structure assigned to low-frequency totally symmetric modes and their overtones/combinations. The Raman spectra have been measured using several excitation wavelengths in pre- and/or near-resonance conditions with respect to the L_a and B_a states. A_1 and a_2 vibrational modes are resonantly enhanced in both cases. Excited-state equilibrium geometries and energies of **1** and **2** have been calculated by means of the MCSCF/CAS ab initio procedure. Franck−Condon factors have been determined coupling structural data with normal mode displacements. On this basis fluorescence and Raman excitation profiles are reasonably well fitted to the experiment. It is concluded that the L_b, L_a, and B_a states of **1** and **2** have equilibrium structures accurately described by the present calculations.

I. Introduction

Electronic spectra of aromatic molecules are characterized by the well-known L_b, L_a, B_a, and B_b bands in the ultraviolet/visible region.[1] Whenever their absorption systems and/or fluorescence emission from the lowest excited state, either L_b or L_a, show clear Franck−Condon envelopes, the band analysis gives clues about the structural changes occurring as a result of the $\pi\pi^*$ excitation, since the intensities depend, among other factors, on the relative displacement between ground and excited-state energy minima.[2] Thus, it has been inferred that the hexagonal structure of benzene expands uniformly in the $S_1(L_b)$ state with the C−C bond increasing by 0.037 Å with respect to the ground-state value,[3,4] whereas in the case of the four independent bonds of naphthalene, two of them, i.e., the 1,2 and the inter-ring bond, stretch by 0.054 and 0.032 Å, respectively, in $S_1(L_b)$ and the other two remain unchanged.[5,6] A more complex variation occurs for the $S_1(L_a)$ state of anthracene consisting of the expansion of the central ring and of the approximate equalization of C−C bonds in the outer rings.[7]

Within this context also the excited states of bridged [$4n + 2$]annulenes ($n = 2,3,4$) have been the subject of considerable interest.[8−12] The four fundamental $\pi\pi^*$ transitions are easily seen in the absorption spectra of bridged [10]- and [14]annulenes.[8,9] The spectral analysis suggests that a strong transannular interaction occurs between bridgehead C atoms.[9] More recently, the $S_1(L_b)$ potential energy surface of 1,6-methano- and 1,6-epoxy-[10]annulene and of **1** was probed by site-selected fluorescence excitation and jet spectroscopy.[10−14] The most active totally symmetric modes of $S_1(L_b)$ tend to flatten the molecular ring and to decrease the transannular interaction. In fact, the calculated $S_1(L_b)$ equilibrium geometry of 1,6-methano- and 1,6-epoxy-[10]annulene has expanded ring size with the 1,6 interannular distance increased by ≈0.1 Å.[11,14] The delicate balance involving interactions between nonbonded atoms, steric strain and aromatic stabilization is expected to have considerable importance also for other $\pi\pi^*$ states. The present paper is concerned with the determination of excited-state geometries of two representative bridged [14]annulenes with an anthracene perimeter, i.e., 1,6:8,13-ethanediylidene[14]annulene and 1,6:8,13-propanediylidene[14]annulene (**1** and **2** in Figure 1, respectively). Fluorescence and Raman data on **1** and **2** have been obtained and related to the structure of the L_a, L_b, and B_a states. In particular, the Raman experiments have been performed in pre- or near-resonance conditions, taking advantage of the circumstance that laser sources with emission wavelength on the onset of the L_a and B_a bands are available.

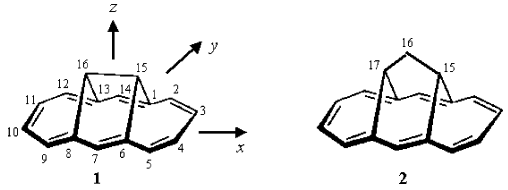

1 **2**

Figure 1. Molecular structures of 1,6:8,13-ethanediylidene[14]annulene (**1**) and 1,6:8,13-propanediylidene[14]annulene (**2**). The common axis reference system and numbering of the ring C atoms are shown only on **1**.

The analysis of the experimental data has been coupled to ab initio calculations of vibrational coordinates and excited-state geometries. Recently, our group has reported on the vibrational spectra of **1** and **2**, fully characterizing the ground-state structures and the normal mode dynamics by means of density functional (DF) calculations.[15] As far as $\pi\pi^*$ states are concerned, a large amount of calculation data has been accumulated over the years dealing with L_b and L_a structures and vertical excitation energies.[6,16−21] In our own work on bridged [10]annulenes,[11,14] the structure of the $S_1(L_b)$ state has been calculated by means of the MCSCF/CAS procedure. Following this approach the optimized strucures of the L_a, L_b, B_a, and B_b states have been determined for both **1** and **2** molecules.

* To whom correspondence should be addressed. E-mail: piero.salvi@unifi.it.

10.1021/jp0474780 CCC: $27.50 © 2004 American Chemical Society
Published on Web 09/10/2004

TABLE 1: Calculated MCSCF/CAS(10,10)/6-31G Structures of the Ground (S_0) and of the Lowest $\pi\pi^*$ States of 1: C−C Bond Lengths (Å) and Distances (Å) between Nonbonded (···) Atoms, Geometrical Indexes A, $|\Delta r_m|$ (Å) and $|\Delta z_m|$ (Å) of Aromaticity as Defined in the Text and Singly Excited Configurations Most Contributing to $\pi\pi^*$ States[a]

	S_0			L_b	L_a	B_a	B_b
	DF/B3-LYP	MC/CAS	exp		MC/CAS		
1,2	1.402	1.398	1.406	1.410	1.384	1.403	1.417
2,3	1.397	1.396	1.381	1.408	1.424	1.402	1.388
3,4	1.415	1.391	1.404	1.383	1.373	1.400	1.408
6,7	1.403	1.403	1.387	1.414	1.410	1.408	1.414
1···6	2.514	2.508	2.469	2.554	2.478	2.552	2.525
1,15	1.518	1.514	1.524	1.513	1.512	1.505	1.514
15,16	1.548	1.547	1.570	1.545	1.545	1.539	1.554
A	0.996	0.998	0.986	0.988	0.957	0.999	0.983
$\|\Delta r_m\|$	0.013	0.006	0.012	0.023	0.028	0.004	0.018
$\|\Delta z_m\|$	0.35	0.35	0.45[b]	0.33 ≈ [(H,L) − (H-1,L + 1)]	0.40 ≈ (H-1,L)	0.30 ≈ [(H-1,L) + (H,L + 1)]	0.35 ≈ [(H,L) + (H-1,L+1)]

[a] For the sake of comparison, DF/B3-LYP/cc-pVDZ results from ref 15 and the experimental geometry of the 15,16-dimethyl derivative of **1** from ref 25 are also reported. In the first column the C,C pairs are numbered as in Figure 1. [b] The calculated value for the 15,16-dimethyl derivative is 0.40 Å.

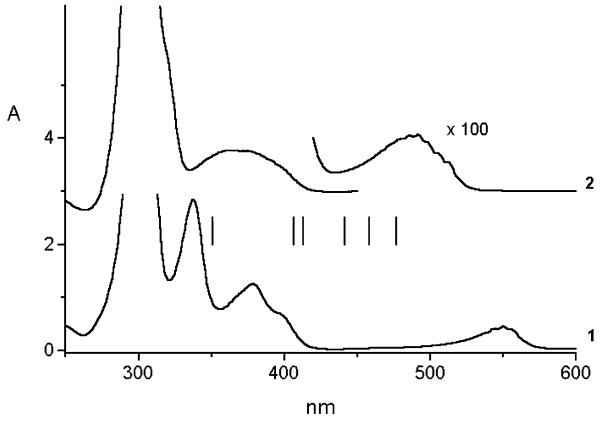

Figure 2. Absorption spectra of **1** and **2** (lower and upper traces, respectively, $c = 5 \times 10^{-4}$ M for **1**; 2×10^{-5}, 2×10^{-3} M for **2** in isopentane/diethyl ether mixture at room temperature). The excitation wavelengths of the Raman spectra are shown on the Figure as vertical lines between the two traces. The spectrum of **2** has been for convenience shifted along the absorbance axis.

II. Experimental Section

The bridged [14]annulenes **1** and **2** were prepared following the reported synthetic routes.[22,23] Purification and recrystallization procedures as well as NMR control spectra were already described.[15] Both samples were stored at −10 °C until use.

The instrumental apparatus for the measurement of fluorescence spectra at low temperature has been described elsewhere.[11] Shortly, rigid glassy isopentane/diethyl ether mixtures (7:3; $c = 10^{-4}$ and 10^{-3} M, for **1** and **2**, to have equal absorbances at the excitation wavelength, 548.4 and 504.6 nm, respectively) are formed by introducing the cell containing the sample under vacuum conditions into a homemade cryostat at liquid-nitrogen temperature. The lines from a N_2-pumped dye laser and from an OPO system pumped by the third harmonic of a Nd:YAG laser were employed for $S_0 \rightarrow S_1$ excitation. The fluorescence signal, dispersed through a Jobin-Yvon double monochromator, is detected by an air-cooled photomultiplier and averaged by the Boxcar (Stanford, mod. SR250). The slit width of the monochromator was ≈ 100 μm, corresponding to a bandwidth of ≈ 5 cm^{-1}.

Solutions of **1** and **2** ($c = 10^{-3}$ M in isopentane/diethyl ether) were freshly prepared for each Raman experiment at room temperature. Six excitation lines, 476.5 and 457.9 nm (Ar^+ laser), 441.6 nm (He−Cd laser), and 413.1, 406.7, and 350.7 nm (Kr^+ laser) were employed. The position of all these lines with respect to the absorption bands of **1** and **2** is shown in Figure 2. According to the band assignment,[8] the excitation lines down to 406.7 nm fall in the preresonance and resonance region with respect to the L_a absorption while the last is at the onset of the B_a absorption, at least for **1**. It was not possible to measure spectra with other Ar^+ and Kr^+ laser lines, due to the large fluorescence emission under which the much weaker Raman signal is buried or severely distorted. No Raman bands of **1** and **2** are observed exciting at 647.1 nm with the red line of the Kr^+ laser. Only polycrystalline samples show appreciable intensity under these conditions.[15] Each solution spectrum was doubled by that of the pure solvent mixture, thus making easier, by comparison, the observation of weak lines of the solute. The Raman spectra were taken with standard collection instrumentation (double monochromator, spectral resolution $\Delta\nu \approx 6$ cm^{-1}, red-extended cooled photomultiplier, photon counting detection system). For all excitation wavelengths, the laser power was kept constant around 40 mW. Solution spectra measured at different times during the experiment did not show any decrease of the Raman signal, indicating that both molecules are stable upon our irradiation conditions. The Raman spectra were mostly measured at room temperature; few of them were also obtained at 77 K.

The absorption spectra of **1** and **2** were measured at room and low temperature on a Cary 5 spectrophotometer with a spectral resolution of 2 nm.

III. Results and Discussion

A. Molecular Structures and Energies. The ab initio optimization of equilibrium geometries has been performed with the program GAMESS for the ground and the lowest $\pi\pi^*$ states.[24] The MCSCF/6-31G wave function for each of these states has been determined following the complete active space (CAS) approach, i.e., considering the occupation by 10 electrons of 10 molecular orbitals (5 occupied and 5 virtual) chosen among those having the largest p_z contribution from the ring C atoms. The total number of excited configurations is 19 404. The overall procedure was successfully adopted in related molecules, 1,6-methano- and 1,6-epoxy-[10]annulene.[11,14] The optimized structures of the ground and of the four excited states which are of interest in the present work are presented in Tables 1 and 2.

TABLE 2: Calculated MCSCF/CAS(10,10)/6-31G Structures of the Ground (S_0) and of the Lowest $\pi\pi^*$ States of 2: C−C Bond Lengths (Å) and Distances (Å) between Nonbonded (···) Atoms, Geometrical Indexes A, $|\Delta r_m|$ (Å) and $|\Delta z_m|$ (Å) of Aromaticity as Defined in the Text and Singly Excited Configurations Most Contributing to $\pi\pi^*$ States[a]

	S_0			L_b	L_a	B_a	B_b
	DF/B3-LYP	MC/CAS	exp		MC/CAS		
1,2	1.415	1.413	1.413	1.420	1.392	1.423	1.418
2,3	1.391	1.388	1.387	1.408	1.422	1.390	1.394
3,4	1.425	1.404	1.414	1.388	1.379	1.411	1.411
6,7	1.404	1.404	1.395	1.416	1.413	1.411	1.410
1···6	2.408	2.408	2.384	2.479	2.386	2.440	2.477
1,15	1.516	1.512	1.517	1.516	1.511	1.513	1.512
15,16	1.523	1.520	1.518	1.522	1.518	1.522	1.522
15···17	2.444	2.443	2.434	2.443	2.448	2.451	2.437
A	0.984	0.989	0.984	0.987	0.971	0.981	0.990
$\|\Delta r_m\|$	0.019	0.014	0.014	0.022	0.025	0.018	0.013
$\|\Delta z_m\|$	0.73	0.75	0.70	0.77 ≈ [(H,L) − (H-1, L + 1)]	0.60 ≈ (H-1,L)	0.80 ≈ [(H-1,L) + (H,L + 1)]	0.79 ≈ [(H,L) + (H-1,L + 1)]

[a] For the sake of comparison, DF/B3-LYP/cc-pVDZ results from ref 15 and the experimental geometry of **2** from ref 26 are also reported. In the first column the C,C pairs are numbered as in Figure 1.

The ground-state structures of **1** and **2** are known to belong to C_{2v} symmetry with small bond alternation along the ring, according to the X-ray diffraction data on **2** and on the 15,16-dimethyl derivative of **1**.[25,26] DF calculations predict for both molecules a C_{2v} geometry in good agreement with experiment.[15] The present results on the ground state of **1** and **2** exhibit the same accuracy. The degree of aromaticity of these structures may be assessed on the basis of geometric criteria proposed in the past years.[27−29] The first is the Julg parameter $A = 1 - (225/n)\sum_i[1 - (r_i/\bar{r})]^2$, a measure of bond length alternation, where n is the number of C−C bonds involved in the conjugation (14 in our case), r_i is the length of the ith C−C bond, and $\bar{r}$ is the mean value.[29] A is unity for the fully delocalized benzene structure ($r_i = \bar{r}$) and zero for the hypothetical bond alternating structure with $r_{C-C} = 1.52$ Å and $r_{C=C} = 1.33$ Å. The second important parameter is $|\Delta r_m|$, the absolute maximum deviation of the C−C bond lengths from the mean. Aromatics have $|\Delta r_m| \leq 0.05$ Å.[27] The two indexes reported in Tables 1 and 2 give evidence of the aromatic character of the two molecules. For non planar bridged annulenes it is useful, to our opinion, to define a third index, $|\Delta z_m|$, which is the absolute maximum difference between the z coordinates of the ring C atoms. From the $|\Delta z_m|$ values of the ground state, it is seen that **1** is less distorted from planarity than **2**, due to the smaller flexibility of the bridge. Considering the three indexes for the excited states of **1**, B_a has the most pronounced aromatic character, all of the C−C bond lengths being almost equal ($A = 0.999$; $|\Delta r_m| = 0.0042$ Å) and the ring less distorted ($|\Delta z_m| = 0.30$ Å). It may be also seen from Table 1 that L_a falls at the other extreme, $A = 0.957$, $|\Delta r_m| = 0.028$ Å, $|\Delta z_{C,max}| = 0.40$ Å. Other structural data of interest are (i) the distance between nonbonded opposite, i.e., 1,6 and 8,13, atoms largely increasing from the ground to the L_b and B states and (ii) the C−C bond lengths at the ring periphery having a stronger variation upon excitation than those at the center. Structural data of **2** have a trend similar to that described for **1** (see Table 2). In addition, the excited states of **2** show a higher distortion from planarity than those of **1**. The B_a state, in particular, is the most distorted among the excited states of **2** while the reverse holds for the B_a state of **1**.

Despite the high number of configurations, the MCSCF wave functions are described to a good approximation as linear combinations of few singly excited configurations, also reported in the tables. For planar aromatics, the most important contributions to L_b, L_a, B_a, and B_b wave functions coming from singly excited configurations are[1] (HOMO,LUMO+1) − (HOMO-1,LUMO), (HOMO,LUMO), (HOMO-1,LUMO+1), and (HOMO, LUMO+1) + (HOMO-1,LUMO), respectively. In our own 6-31G calculation the HOMO orbital of **1**/**2** correlates with (HOMO-1) of anthracene [and (HOMO-1) with HOMO] for symmetry reasons so that the excited configurations do not appear in the usual form but rather with the HOMO/(HOMO-1) interchange. This interesting result may be rationalized on a simple basis, i.e., applying the PMO treatment[30] to anthracene and to **1**/**2**, considered as systems formally derived from cyclotetradecaene ($C_{14}H_{14}$) by cross-linking and bridging, respectively.[1] Each π and π^* orbital energy of the regular $C_{14}H_{14}$ polygon is by symmetry doubly degenerate (apart the lowest and the highest, which are nondegenerate) and one component of the degenerate pair is symmetric (s), whereas the other is antisymmetric (a) with respect to an appropriate vertical nodal plane.[1] The two perturbations, cross-linking and bridging, are classified as odd and even,[31] respectively. In addition to the even bridging perturbation, in **1**/**2**, we have the odd perturbation due to the transannular interaction. The former is however much stronger than the latter so that the net perturbation is even. The MOs of $C_{14}H_{14}$ may be correlated[1] to those of anthracene and **1**/**2** on the basis of the Hückel approximation and considering the pairing theorem of alternant hydrocarbons.[32,33] Due to the perturbation (i) the HOMO pair as well as the LUMO pair of $C_{14}H_{14}$ split into two nondegenerate orbitals and due to the symmetry label of the perturbation (ii) the energy ordering in anthracene (odd perturbed $C_{14}H_{14}$) is $(HOMO\text{-}1)_a < HOMO_s < LUMO_s < (LUMO+1)_a$ and in **1**/**2** (even perturbed $C_{14}H_{14}$) $(HOMO\text{-}1)_s < HOMO_a < LUMO_s < (LUMO+1)_a$. It is concluded that HOMO/HOMO-1 crossing occurs on going from anthracene to **1**/**2**.

The vertical excitation energies and the oscillator strengths of the transitions from the ground-state minimum to the four excited states have been calculated. The MCSCF/CAS(10,10)/6-31G energies at the ground-state equilibrium geometry were corrected to second-order applying the multireference perturbation treatment (MC/QDPT)[34,35] included in the GAMESS program. The perturbative term is intended to account for the $\sigma - \pi$ correlation energy and has already given good results in a similar case.[12] In the absorption spectra of **1** and **2** below 4.5 eV up to seven electronic transitions have been assigned, though not all as $\pi\pi^*$ transitions.[8] Four $\pi\pi^*$ bands have been recognized[8] whose energies and intensities are listed together with the calculated data in Table 3. Vertical excitation energies are in good agreement with experimental values. In the case of the B_b band of **2** only, the discrepancy between calculated and

TABLE 3: Calculated (MC/CAS(10,10)/QDPT/6-31G) and Experimental Vertical Transition Energies (ΔE, EV) and Oscillator Strengths f from the Ground to the Lowest $\pi\pi^*$ States of 1 and 2[a]

	1				2			
	ΔE		f		ΔE		f	
	calc	exp	calc	exp	calc	exp	calc	exp
L_b	1.61	2.23	0.006	0.02	2.71	2.42	0.001	0.004
L_a	3.30	3.07	0.27	0.02	3.42	3.10	0.21	0.06
B_a	3.41	3.65	0.60	0.15	3.77	3.85	0.67	0.15
B_b	3.92	3.99	1.21	1.10	7.70	4.09	2.18	1.60

[a] The experimental values are from ref 8.

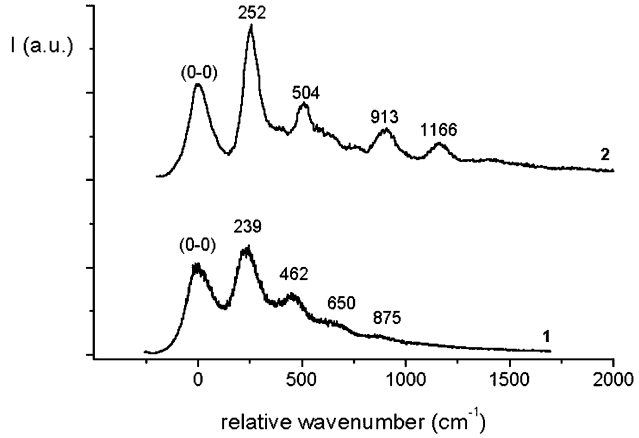

Figure 3. Fluorescence spectra of **1** and **2** (lower and upper traces, respectively) with abscissa axis relative to the (0−0) transition energy, 17 965 cm^{-1} for **1** and 19 495 cm^{-1} for **2**. The experimental conditions are $c = 10^{-4}$ and 10^{-3} M in isopentane-diethyl ether mixture for **1** and **2**, respectively, T = 77 K, excitation wavelength 548.4 nm for **1** and 504.6 nm for **2**. The vibrational spacings (cm^{-1}) from the origin,(0−0), band are indicated on the figure.

observed values is anomalously large, much probably due to the occurrence of an intruder state.[24]

B. $S_1 \rightarrow S_0$ Fluorescence. The low-temperature fluorescence spectra of **1** and **2**, shown in Figure 3, have been measured exciting into the first vibronic band of the L_b absorption system, i.e., at 548.4 nm for **1** and at 504.6 nm for **2**. The two spectra have been already reported and interpreted in terms of Franck−Condon allowed transitions.[8] The fluorescence data of interest for the present work are discussed in detail in this section.

The lowest $\pi\pi^*$ states of molecules such as **1** and **2**, having C_{2v} symmetry,[15,25,26] belong to $B_1(L_b)$, $B_2(L_a)$, $B_2(B_a)$, and $B_1(B_b)$ symmetry species,[8] in order of increasing energy (see Figure 2 and Table 3). The purely electronic $S_1 \rightarrow S_0$ transition is allowed and observed at 17 965 cm^{-1} for **1** and at 19 495 cm^{-1} for **2**. The former is red-shifted by 35 cm^{-1} with respect to the absorption origin, 17 990 cm^{-1}, whereas the latter is red-shifted by 45 cm^{-1}, the absorption origin being at 19 540 cm^{-1}. The (0−0) emissions are partly reabsorbed, as it may be also guessed from their slightly asymmetric band shapes. Though the reabsorption path length is difficult to assess quantitatively, a reasonable estimate, given our experimental conditions (45° incidence direction on a 0.2 cm cell), is ≤ 0.1 cm. The fluorescence spectrum of **2** is structured with bands 252, 389, 504, 647, 750, 913, and 1166 cm^{-1} from the origin band, tentatively assigned to overtones of the 252 cm^{-1} mode and combinations with the 389 cm^{-1} mode. This preliminary assignment is to some degree oversimplified since for several bands two (or more) vibronic transitions may contribute to the observed band. The 252 cm^{-1} mode describing ring expansion

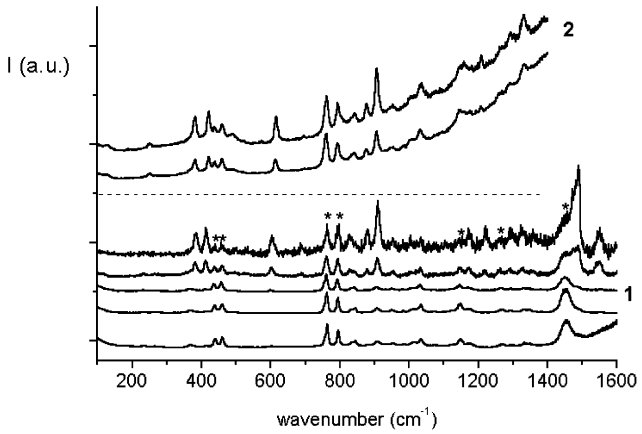

Figure 4. Raman spectra of **1** and **2** (lower five and upper two traces, respectively, $c = 10^{-3}$ M in isopentane/diethyl ether mixture, room temperature). The excitation lines are, from bottom to top, 476.5, 457.9, 441.6, 413.1, and 406.7 nm for **1** and 413.1 and 406.7 nm for **2**. The most intense solvent bands are indicated by asterisks in the 406.7 nm spectrum. For the sake of clarity the intensity of the solvent band 460 cm^{-1} has been set to a common value in all the spectra of the figure.

is active also in the nonresonant Raman spectrum of **2**.[15] The more diffuse spectrum of **1** has a limited number of vibronic bands (239, 462, 650, and 875 cm^{-1}) among which the first, corresponding to the 252 cm^{-1} mode of **2**, has the strongest activity.

C. Raman Scattering. Making reference, for the sake of simplicity, to the theoretical model most commonly used in the interpretation of RR data,[36−39] two terms, the so-called A and B terms, predominantly contribute to the polarizability tensor of the vibrational transition $|gi\rangle \rightarrow |gf\rangle$, when the excitation energy ω_{exc} approaches a particular transition energy $\omega_{ev,gi}$. The A term accounts for intensity enhancement of a_1 fundamentals through Franck−Condon coupling while the second is responsible for that of nontotally symmetric fundamentals (and for an additional contribution to intensities of totally symmetric fundamentals) through vibronic coupling of the final state with excited states of appropriate symmetry. The largest contribution to Raman scattering with excitation wavelength approaching the L_a band is expected from totally symmetric fundamentals through the A term. Vibronic coupling of L_a with the strongly absorbing B_b state enhances the activity of a_2 modes. The L_a−B_b coupling is responsible for the activity of b_{3g} modes in naphthalene and anthracene.[40,41] As to the resonance enhancement due to the B_a band, only the A term should reasonably affect the a_1 intensity. Modes of a_2 symmetry may be observed through B_a−B_b coupling.

The Raman spectra of the solution 10^{-3} M of **1** and **2** in isopentane/diethyl ether mixture in preresonance and near-resonance conditions with respect to L_a band are collected in Figure 4. Considering first the Raman spectra of **1**, it is easily seen by visual inspection that the peaks 382, 412, 602, 688, 878, 909, 1171, and 1219 cm^{-1} and the two unresolved Raman doublets around 1480 and 1550 cm^{-1} are enhanced approaching the L_a band. On the basis of the vibrational assignment[15] these modes are totally symmetric, except the 1171 cm^{-1} and one component of each doublet, of a_2 symmetry. The Raman excitation profiles (REP) have been determined with the following procedure. Preliminarly, the solvent Raman spectrum has been fitted with bands of mixed (Gaussian and Lorentzian) character. The fitting was repeated for the solution spectrum assuming no variation of the relative band intensities for the solvent in the solution. This made it possible to evaluate intensities even when solute and solvent bands badly overlap or when the former are weak. A sample of our fitting procedure

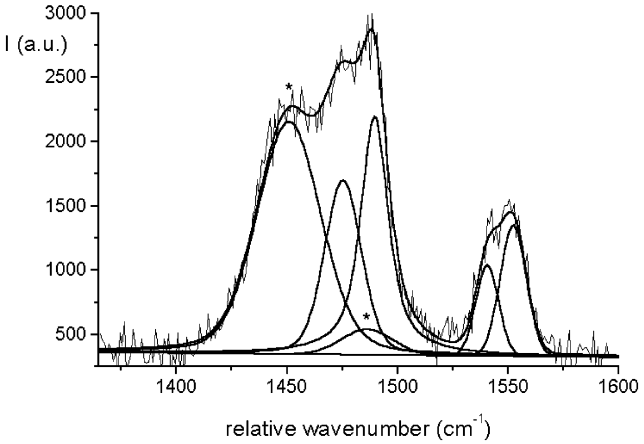

Figure 5. Fitting of the Raman spectrum of **1** in the spectral region 1400−1600 cm^{-1} exciting at 413.1 nm. The two solvent bands observed at 1450 cm^{-1} (strong) and at 1486 cm^{-1} (very weak) are denoted with asterisks.

is displayed in Figure 5. Then, correction factors to the intensity of each solute band were applied as recommended in a recent report.[42] The solvent 460, 761, 1146, 1261, and 1451 cm^{-1} intensities at each excitation wavelength were normalized to their counterparts at 413.1 nm and the same correction applied to solute bands in their proximity. This accounts for self-absorption and differences in the optical path length from one experiment to another. A second correction, due to the ω^4 factor, was obtained for each solute band considering close lying solvent bands. All of the observed Raman fundamentals and their intensities, increasing up to 2 orders of magnitude as a function of the wavelength, are collected in Table 4. REP's of two representative modes, 382 (a_1) and 1489 (a_1) cm^{-1}, are shown in Figure 6.

The low-frequency a_1 modes 382, 412 and 602 cm^{-1} couple favorably the ground with the L_a geometry. The normal displacements, derived from density functional calculations and substantially located on the ring,[15] do not lead to a structure more planar than in S_0. On the other hand, the 234 cm^{-1} mode, where the ring motion is more effectively coupled with that of the ethane bridge,[15] is not enhanced. This mode, particularly active in the fluorescence spectrum and in the $S_0 \rightarrow S_1$ fluorescence excitation spectrum,[10] expands and flattens the ring while increasing the bridge distance from the ring.[10,15] Qualitatively, the two results suggest a less extended delocalization of π electrons in L_a than in L_b, in reasonable agreement with calculated structures.

The comparison of data on **1** with resonance Raman results on anthracene[41,43] should be also considered. Preresonance enhancement, up to 457.9 nm excitation wavelength, of anthracene a_g and b_{1g} vibrations (reference system: *x* and *y*, in-plane long and short axes, respectively; *z*, out-of-plane axis) has been reported.[41,43] Among a_g modes, those at 1403 and 1556 cm^{-1} show the most pronounced effect.[41] They correspond to the 1361 and 1489 cm^{-1} modes of **1**, according to our assignment.[15] It should be noted that while the 1403 cm^{-1} band of anthracene is strongly active far from resonance, the 1361 cm^{-1} band of **1** is weak off resonance. The intrinsic weakness of this band is related to the nature of the mode, substantially localized in **1** on the rigid CCC bridges rather than on the polarizable inter-ring CC bonds such as in anthracene.[15] Among anthracene b_{1g} modes, that at 1630 cm^{-1} is reported to have the largest enhancement.[41] This corresponds to the 1541 cm^{-1} a_2 mode of **1** with vanishing Raman intensity off resonance. A second peak at 1550 cm^{-1}, of a_1 symmetry, is correlated with

TABLE 4: Relative Raman Intensities, (I_R), of a_1 and a_2 Modes (ω, cm^{-1}) of 1 and 2 as a Function of the Excitation Wavelength (nm) Approaching the L_a Absorption Band[a]

	I_R				
	exc(nm)				
ω	476.5	457.9	441.6	413.1	406.7
			1		
234(a_1)	2005	1136	1916	4022	3147
382(a_1)	180	647	1108	20646	42491
412(a_1)	663	1300	1093	19761	24410
494(a_2)		647		5780	10921
602(a_1)	2550	1753	4727	24258	44816
688(a_1)	124	154	11	4249	12326
734(a_1)	147	89	29	1660	3571
828(a_1)	3	438	1063	9061	21142
878(a_1)	480	742	1631	14116	16549
909(a_1)	625	5338	888	13633	42814
1171(a_2)	390	78	734	6497	19810
1219(a_1)	10	550	972	10401	28047
1289(b_1)	8	2035	721	8519	13110
1327(a_2)	215	318	1118	6093	9045
1361(a_1)	2677	1465	521	5016	9075
1475(a_2)	3580	2849	10248	126428	188902
1489(a_1)	5484	6701	18476	158945	293538
1541(a_2)			233	35683	71667
1550(a_1)			7608	58878	98194
			2		
129(a_2)				42661	85923
248(a_1)				58997	78374
379(a_1)				198964	312168
419(a_1)				155238	286698
486(a_2)				156449	154486
613(a_1)				376293	689840
875(a_1)				70670	159326
905(a_1)				153604	364719

[a] The intensities have been determined through the fitting procedure described in the text.

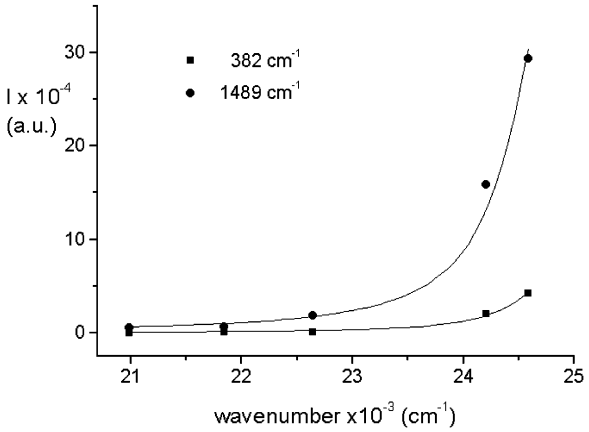

Figure 6. Excitation profiles of the a_1 modes 382 and 1489 cm^{-1} (intensities relative to that of the 460 cm^{-1} solvent band exciting at 413.1 nm) as a function of the excitation energy approaching the L_a state. Each excitation profile has been fitted to eq 1 with (0−0) transition energy, i.e., the $\omega_{e,0;g,0}$ quantity of the text, taken from ref 10 equal to 24 800 cm^{-1}, with $\gamma = 420$ cm^{-1} and $\Gamma = 0.0026$ cm^{-1}.

the 1480 cm^{-1} a_{1g} mode of anthracene.[15] Finally, the a_2 mode of **1** occurring at 1475 cm^{-1} with large off resonance Raman activity, correlates with the b_{1g} mode at 1574 cm^{-1}.

As to **2**, a smaller set of Raman data has been obtained. Since **2** is highly fluorescent and the first absorption region of **2** is blue-shifted with respect to **1** (see Figure 2) the spectra observed with the highest excitation wavelengths, up to 441.6 nm, overlap with the fluorescence spectrum and, as a result, are strongly distorted. Only the Raman spectra exciting at 413.1 and 406.7 nm, i.e., on the onset of the L_a absorption, are significant for the present study (see Figure 4, upper two traces). The relative

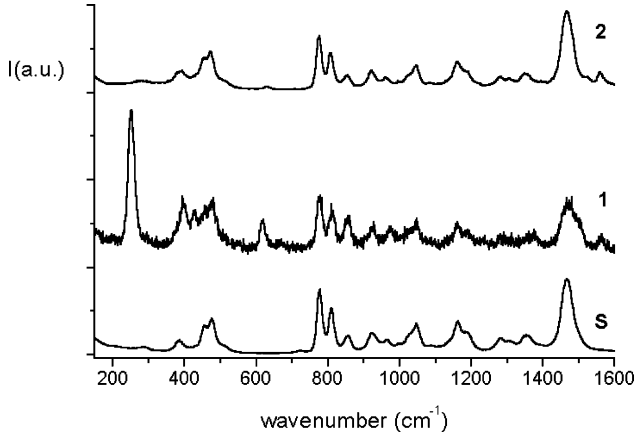

Figure 7. Raman spectra of **1** and **2** (middle and upper trace, respectively, $c = 10^{-3}$ M in isopentane/diethyl ether mixture, room temperature) compared with the spectrum of the solvent mixture (**S**, lower trace) exciting at 350.7 nm. The intensity of the solvent band 460 cm^{-1} has been set to a common value in all the spectra of the figure.

intensities of the Raman bands have been found by means of the fitting procedure and collected in Table 4. Modes of a_1 symmetry 248, 379, 419, 613, 875 and 905 cm^{-1} are enhanced relative to the solvent bands 460 and 761 cm^{-1}. Additional peaks are observed at 129 cm^{-1} and at 486 cm^{-1}, assigned to modes of a_2 symmetry.[15] Above 1000 cm^{-1} several other Raman lines [1156(a_2), 1206(a_1), 1330(a_1), 1469(a_1), 1513(a_1), 1545(a_2) cm^{-1}] are observed for which however it was difficult to evaluate the intensity due to the band distortion.

The Raman spectra of **1** and **2** exciting at 350.7 nm are shown in Figure 7. As seen from Figure 2 the spectrum of **1** is in preresonance with the B_a state while, as to **2**, the excitation wavelength has a larger gap with the same state. The spectrum of **1** is dominated by the 234 cm^{-1} band, in remarkable contrast with the weakness of the same band approaching L_a (see Figure 4). This suggests that the corresponding coordinate favors the structural change from the ground to the B_a state. Considering the normal displacements,[15] the B_a equilibrium geometry has more balanced C−C bond lengths and a more planar ring structure than in the ground state. As to **2**, the spectrum of the solution is not much different from that of the solvent in the same conditions. The resonance effect on the Raman modes is moderate and probably due more to the lower L_a state than to the higher B_a state. The only clearly observed bands are at 379 (a_1), 613 (a_1), 1513 (a_1), and 1545 (a_2) cm^{-1} while the Raman peak at 248 cm^{-1} is barely seen.

D. Model Calculations. Franck−Condon factors are the key quantities to calculate fluorescence and Raman excitation profiles.[2,7]

Starting with the fluorescence emission, the intensity $I(0_{Lb} \rightarrow v_{p,g})$ of the allowed transition from the vibrationless $|0_{Lb}\rangle$ level of the excited L_b state to the $|v_{p,g}\rangle$ ground (g) state level of the totally symmetric p coordinate relative to that of the $|0_{Lb}\rangle \rightarrow |0_g\rangle$ transition is given by[1]

$$\frac{I(0_{Lb} \rightarrow v_{p,g})}{I(0_{Lb} \rightarrow 0_g)} = \frac{|\langle 0_{Lb}|v_{p,g}\rangle|^2}{|\langle 0_{Lb}|0_g\rangle|^2}$$

where $|0_{Lb}\rangle$, $|v_{p,g}\rangle$, $|0_g\rangle$ are vibrational wave functions, 0-th and v-th level, respectively, of the p coordinate associated with the L_b and the ground state. Assuming that the excited-state potential is not distorted relative to that of the ground state ($\omega_{p,Lb} = \omega_{p,g} = \omega_p$; cm^{-1}) and neglecting the mixing of totally symmetric modes upon electronic excitation, the Franck−Condon factor $\langle 0_{Lb}|v_{p,g}\rangle$ depends only on the displacement parameter Δ_p, i.e., on the shift of the L_b minimum with respect to that of the ground-state projected along the pth coordinate. Under these circumstances Franck−Condon factors are obtained from the Manneback recurrence relations[44]

$$\langle 0_{Lb}|v_{p,g}+1\rangle = -\langle 0_g|v_{p,Lb}+1\rangle = \frac{\Delta_p}{v_p+1}\langle 0_{Lb}|v_{p,g}\rangle$$

It may be shown[2] that

$$\Delta_p = 0.172\sqrt{\frac{\omega_p}{2}}(\mathbf{X}_{Lb} - \mathbf{X}_g)\mathbf{m}^{1/2}\pounds_p$$

where $\mathbf{X}_{Lb}$ and $\mathbf{X}_g$ are the $3n$ equilibrium coordinates of the L_b and g states, $\mathbf{m}$ the diagonal $3n \times 3n$ matrix of the atomic masses, $\pounds_p$ the $3n$-dimensional Cartesian eigenvector of the p mode, $v_{p,Lb} = v_{p,g} = v_p$ the vibrational level and 0.172 a dimensional ($g^{-1/2}$ $cm^{-1/2}$) factor equal to $[4\pi^2 c/(hN)]^{1/2} \times 10^8$.

The Δ_p parameters have been calculated from the known MCSCF equilibrium structures of the g and L_b states (see Tables 1 and 2) and from the Cartesian displacements of the totally symmetric modes, 18 for **1** and 20 for **2**, having excluded from this analysis C−H stretchings, for the sake of simplicity. Normal modes of **1** and **2** obtained by means of the DF calculation,[15] when coupled with MCSCF data, were unable to give Franck−Condon intensities matching closely the fluorescence profiles. We have then repeated the normal mode calculation starting with the RHF wave function and using for self-consistency the 6-31G basis set. The frequencies have been correlated with (i) the DF values using as a criterion the similarity of Cartesian displacements and with (ii) the DF-correlated observed frequencies, scaling the 6-31G values with the factor 0.909 for **1** and 0.890 for **2**. The Franck−Condon factors of all these fundamentals are in Tables 5 and 6. As to the L_b state, the Δ values of the 234 cm^{-1} (**1**) and of the 248 cm^{-1} (**2**) modes are by far predominant, in excellent agreement with the fluorescence results. Further, an intensity calculation has been set to reproduce the fluorescence spectra of **1** and **2** considering the contribution

TABLE 5: Franck−Condon Displacement Factors Δ of Totally Symmetric Modes of 1 Relative to the L_b, L_a, and B_a States[a]

				L_a			B_a		
ω			L_b		$\lvert\Delta\rvert/\lvert\Delta_{382}\rvert$			$\lvert\Delta\rvert/\lvert\Delta_{382}\rvert$	
DF[b]	RHF[c]	exp[d]	Δ	Δ	calc	exp	Δ	calc	exp
99	101	138	−0.105	1.394			−0.065		
232	241	234	−0.813	0.750	0.97	0.29	−1.006	3.25	4.25
382	375	382	0.526	0.771	1.	1.	0.309	1.	1.
415	415	412	0.347	0.752	0.97	0.61	0.287	0.93	0.61
594	591	602	−0.294	−0.113	0.15	0.67	−0.045	0.14	1.27
692	702	688	−0.030	−0.251	0.32	0.32	−0.041	0.13	0.04
730	756	734	0.084	0.123	0.16	0.16	−0.006	0.2	0.1
823	825	828	−0.121	−0.245	0.32	0.35	−0.352	1.14	0.29
882	869	878	0.033	0.050	0.06	0.27	−0.024	0.07	0.18
915	962	909	0.105	0.365	0.47	0.45	0.106	0.34	0.18
959	1014	959	0.002	−0.154			−0.094		
998	1074	1001	−0.092	0.002			−0.125		
1194	1238	1206	0.027	−0.053			0.090		
1227	1262	1219	−0.113	0.073	0.09	0.28	−0.046	0.15	0.18
1337	1369	1327	0.053	−0.034	0.04	0.13	0.038	0.12	0.28
1351	1378	1361	0.159	−0.034	0.04	0.16	0.106	0.34	0.28
1501	1539	1489	0.040	−0.224	0.29	0.77	−0.022	0.07	0.61
1560	1585	1550	0.221	0.585	0.76	0.39	−0.080	0.26	0.34

[a] The calculated and observed $|\Delta|/|\Delta_{382}|$ ratios for the L_a and B_a states are reported using eq 2 of the text. [b] From ref 15. [c] Present 6-31G results with scaling factor 0.909. [d] 138, 959, 1001, and 1206 cm^{-1}, observed values relative to the polycrystalline sample.

TABLE 6: Franck−Condon Displacement Factors Δ of Totally Symmetric Modes of 2 Relative to the L_b, L_a, and B_a States[a]

ω			L_b	L_a			B_a		
					$\lvert\Delta\rvert/\lvert\Delta_{379}\rvert$			$\lvert\Delta\rvert/\lvert\Delta_{379}\rvert$	
DF[b]	RHF[c]	exp[d]	Δ	Δ	calc	exp	Δ	calc	exp
118	122	138	−0.119	1.516			−0.332		
250	246	248	0.850	−0.489	0.46	0.76	1.000		
381	387	379	−0.526	1.055	1.	1.	−0.552	1.	1.
424	421	419	0.455	0.963	0.91	0.87	0.142		
577	577	572	−0.081	−0.034			−0.063		
610	609	613	0.386	0.207	0.19	0.93	0.124	0.22	0.25
689	699	693	0.018	−0.237			0.067		
754	775	761	−0.252	−0.423			−0.280		
881	920	875	0.158	0.199	0.19	0.31	0.111		
912	940	905	0.089	0.175	0.16	0.46	−0.182		
938	972	944	−0.069	0.189			−0.118		
970	978	979	0.106	−0.464			−0.108		
994	989	1004	0.025	0.172			−0.112		
1211	1221	1206	−0.155	−0.034			−0.002		
1277	1272	1277	−0.063	0.176			−0.066		
1324	1340	1330	0.020	0.143			−0.073		
1376	1385	1403	−0.067	0.071			−0.072		
1426	1474	1451	−0.156	−0.272			0.018		
1487	1479	1469	0.250	0.351			−0.015		
1510	1504	1513	−0.073	0.166			0.012	0.02	0.16

[a] The calculated and observed $|\Delta|/|\Delta_{382}|$ ratios for the L_a and B_a states are reported using eq 2 of the text. [a] From ref 15. [b] Present 6-31G results with scaling factor 0.890. [c] 138, 761, 944, 979, 1004, 1277, 1403, and 1451 cm^{-1}, observed values relative to the polycrystalline sample.

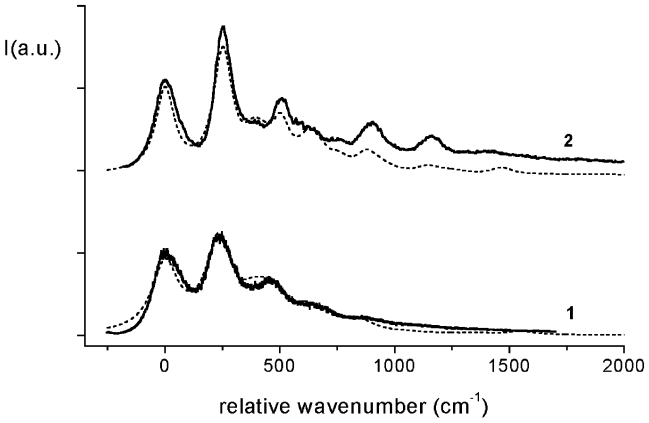

Figure 8. Observed and calculated fluorescence spectra of **1** and **2** (lower and upper traces, respectively). The calculated spectra (dashed lines) have been obtained using the Franck−Condon factors of Tables 5 and 6, taking into account the partial reabsorption of the (0−0) band and reducing the Δ values of all the fundamentals, except 234 (**1**) and 248 (**2**) cm^{-1}, by the factor $\sqrt{2}$. All of the vibronic transitions have been inhomogeneously broadened with γ(HWHM) = 70 and 50 cm^{-1} for **1** and **2**, respectively.

(i) from all fundamentals with an intensity ratio $I(0_{Lb} \rightarrow 1_g)/I(0_{Lb} \rightarrow 0_g) \geq 0.05$, (ii) from the 234 cm^{-1} (**1**) and 248 cm^{-1} (**2**) overtones (up to the third), and (iii) from the combinations of these modes (and their overtones) with the 382, 412, and 602 cm^{-1} (**1**) and with the 379, 419, and 613 cm^{-1} (**2**) modes. The inhomogeneous broadening γ of each line and the partial reabsorption of the (0−0) origin band have been considered. The fluorescence profiles are plausibly reproduced if the Δ quantities relative to the 382, 412, and 602 cm^{-1} modes of **1** and of the 379, 419, and 613 cm^{-1} modes of **2** are partially reduced with respect to those of the 234 cm^{-1} (**1**) and 248 cm^{-1} (**2**) modes. In other words, upon excitation to the L_b state the molecular geometry of **1** (**2**) distorts along the 234 (248) cm^{-1} coordinate slightly more than predicted by the calculated structures. In Figure 8, a fitting calculation is shown where γ has been taken equal to 70 and 50 cm^{-1} for **1** and **2**, respectively, and Δ for all the above-mentioned modes is reduced by a factor of $\sqrt{2}$.

Let us now turn the attention to the Raman spectra. It is, first of all, an experimental result that no overtone or combination mode is active in these spectra approaching either the L_a or the B_a state. This suggests that all Δ_p's relative to the two excited states are not larger than unity. The case of A-term scattering in the $\Delta_p < 1$ regime has been discussed elsewhere.[39,45] In this approximation, it is possible to restrict the summation over the vibronic states of the resonant state to the first two, i.e., $v = 0$ and 1, for the intensity calculation. Allowing for a common homogeneous (Γ; HWHM; cm^{-1}) and inhomogeneous (γ; HWHM; cm^{-1}) broadening of the (0−0) and (0−1) lines,[46] the excitation profile of the *p*th totally symmetric fundamental as a function of the excitation energy $\omega_{exc}(cm^{-1})$ is proportional to the expression[39,45]

$$I_{1p,g;0,g} \propto (\omega_{exc} - \omega_p)^4 \times (\mu_y^o)^4 \times \Delta_p^2 \times \omega_p^2 \times \{(\Sigma/\Gamma)[\omega_0^2 + \omega_{1,p}^2 + 2\Sigma^2][(\omega_{1,p} - \omega_0)^2 + 4\Gamma^2] - 2[\omega_0\omega_{1,p} + \Sigma^2][(\omega_{1,p} - \omega_0)^2 + 4\Gamma\Sigma]\}/\{(\omega_0^2 + \Sigma^2)(\omega_{1,p}^2 + \Sigma^2)[(\omega_{1,p} - \omega_0)^2 + 4\Gamma^2]\} \quad (1)$$

where $I_{1p,g;0,g}$ is the Raman intensity of the *p*th fundamental, $\omega_0 = \omega_{0,e;0,g} - \omega_{exc}$, $\omega_{1,p} = \omega_{1p,e;0,g} - \omega_{exc}$, $\Sigma = \Gamma + \gamma$ and the subscript *e* stands for L_a or B_a (thus giving $(\mu_y^o)^4$ in both cases). It is also possible to extract the ratio of the absolute Δ_p quantities using the relation[39,45]

$$\frac{|\Delta_p|}{|\Delta_{p'}|} = \left(\frac{I_{1p,g;0,g} \times \omega_{p'}^2}{I_{1p',g;0,g} \times \omega_p^2}\right)^{1/2} \quad (2)$$

Δ values between the ground and the L_a state have been calculated following the same procedure outlined for the L_b state and collected in Tables 5 and 6 for **1** and **2**, respectively. It is seen that almost all Δ's are smaller than unity. Only the lowest vibrational mode, 138 cm^{-1} for both **1** and **2**, is associated with Δ values well above unity. Considering the intensity data of the totally symmetric **1** modes in Table 4, a fitting has been attempted with a fixed value of the (0−0) transition energy, i.e., $\omega_{0,e;0,g}$, equal to 24 800 cm^{-1}, as reported,[8] and three parameters, γ and Γ, independent of the vibronic line, and the ratio Δ_p/Δ_{382}, taking as reference the 382 cm^{-1} mode. All the REP's have been expressed with $\gamma = 420$ cm^{-1} and $\Gamma = 0.0026$ cm^{-1} and the ratios Δ_p/Δ_{382} reported in Table 5. The fitting for the 382 and 1489 cm^{-1} modes is shown in Figure 6. The comparison between observed and calculated ratios is surprisingly good for most of the resonance enhanced modes of **1** (see Table 5). The whole procedure has been applied to **2**. The results are probably affected by a larger uncertainty due to the fact that reliable data have been obtained only for two excitation lines, 413.1 and 406.7 nm. Nevertheless the general fair agreement of Δ ratios is conserved. It is however evident that the large Δ value for the 138 cm^{-1} mode is at variance with the data of **1** and **2** in resonance with the L_a state. In the low-frequency region of the Raman spectrum at 77 K (not shown) one weak band of **1** occurs at 122 cm^{-1} while in that of **2** at room-temperature one band is observed at 129 cm^{-1}. Both have been however assigned to the a_2 symmetry in a previous calculation,[15] with resonance enhancement due to the L_a/B_b coupling. On the other hand, a difference between calculated and observed $|\Delta|/|\Delta_{382}|$ ratios is found for the 234, 602, 1489, and 1550 cm^{-1} modes (see Table 5). This may indicate that mode mixing between pairs of coordinates (234 and 602 cm^{-1};

1489 and 1550 cm^{-1}) occurs in the excited state determining an intensity transfer from one mode to the other. It is tempting to assume that also the lowest a_1 coordinate mixes with several others and that this affects heavily the intensity redistribution.

The Δ displacements of **1** and **2** relative to the B_a state are quite similar, as it is seen from Tables 5 and 6. On the whole they are much less than unity, apart from those of the 234 (**1**) and 248 (**2**) cm^{-1} modes, around unity. It is therefore confirmed by the present calculation that the B_a geometry of **1** is mostly determined by the molecular displacement along the 234 cm^{-1} coordinate, in excellent agreement with the experimental spectrum (λ_{exc} = 350.7 nm) where this mode has by far the largest enhancement. The ratios $|\Delta|/|\Delta_{382}|$ at 350.7 nm compare reasonably with ratios derived from ab initio data, except for the 602/828 cm^{-1} pair for which the discrepancy is tentatively ascribed, as in the previous case, to mixing of the two pair components in the excited state. Despite the similarity of Franck−Condon factors the Raman spectrum of **2** with 350.7 nm excitation wavelength exhibits several differences with respect to that of **1**, as already noted, the main being the vanishing intensity of the 248 cm^{-1} mode and a general weakening of the resonance effect for all of the other modes. Two concomitant factors may be envisaged for this behavior: (i) the gap between the excitation and the B_a energy, larger in **2** than in **1**, and (ii) a weak resonance effect due to the lower L_a state, negligible for **1** while still present for **2** because of the difference of the oscillator strengths (see Table 3).

IV. Conclusions

In this paper, excited states geometries of bridged [14]annulenes **1** and **2** have been investigated coupling fluorescence and Raman data with results from ab initio calculations. In particular, Raman data in pre- and near-resonance conditions with respect to the L_a and B_a states have given information about the equilibrium configuration of these states. Raman experiments with excitation resonant with the $S_2(L_a)$ state have been reported only for naphthalene[40] and benzene.[47] To the best of our knowledge, no Raman work has addressed the issue of excitation into the B_a state. It turns out from this work that the L_b and B_a geometries are appreciably distorted relative to the ground-state structure and characterized by a more planar ring arrangement and a smaller alternation of C−C ring bond lengths. In contrast, the L_a geometry has increased bond alternation and non bonded 1···6 (and 8···13) atoms in closer contact than in the ground state.

Calculations on the excited state structure of aromatics are usually focused on the lowest L_a and L_b states.[6,18,20,21] In this study the calculation was extended to the B_a and B_b states, increasing the knowledge on these systems. The agreement between experiment and calculation with reference to B_a state give confidence also to our prediction on the B_b structure.

Finally, it should be stressed that the present work deals with the equilibrium geometries of $\pi\pi^*$ states. From a dynamical point of view it is of interest the dependence of their potential energy on the CH_2 detachment from the ring. Work is in progress in our laboratory on this issue.

Acknowledgment. This work was supported by the Italian Consiglio Nazionale delle Ricerche (CNR) and Ministero dell'Universita' e della Ricerca Scientifica e Tecnologica (MIUR). The authors gratefully thank Prof. G. Hohlneicher (University of Köln, Germany) for critical reading of the manuscript.

References and Notes

(1) Klessinger, M.; Michl, J. *Excited states and photochemistry of organic molecules*; VCH Publishers: New York, 1994.
(2) Siebrand, W. M.; Zgierski, M. Z. In *Excited states*; Lim, E. C., Ed.; Academic Press: New York, 1979; Vol. 4, pp 1−135.
(3) Craig, D. P. *J. Chem. Soc., London* **1950**, 2146−2151.
(4) Ziegler, L. D.; Hudson, B. S. In *Excited states*; Lim, E. C., Ed.; Academic Press: New York, 1982; Vol. 5, pP 42−140.
(5) Innes, K. K. In *Excited states*; Lim, E. C., Ed.; Academic Press: New York, 1975; Vol. 2, pp 1−32.
(6) Swiderek, P.; Hohlneicher, G.; Maluendes, S. A.; Dupuis, M. *J. Chem. Phys.* **1993**, *98*, 974−987.
(7) Zerbetto, F.; Zgierski, M. Z. *Chem. Phys.* **1988**, *127*, 17−29.
(8) Kolc, J.; Michl, J.; Vogel, E. *J. Am. Chem. Soc.* **1976**, *98*, 3935−3948.
(9) Dewey, H. J.; Deger, H.; Frolich, W.; Dick, B.; Klingensmith, K. A.; Hohlneicher, G.; Vogel, E.; Michl, J. *J. Am. Chem. Soc.* **1980**, *102*, 6412−6417.
(10) Klingensmith, K. A.; Dewey, H. J.; Vogel, E.; Michl, J. *J. Am. Chem. Soc.* **1989**, *111*, 1539−1546.
(11) Catani, L.; Gellini, C.; Salvi, P. R. *J. Phys. Chem. A* **1998**, *102*, 1945−1953.
(12) Catani, L.; Gellini, C.; Moroni, L.; Salvi, P. R. *J. Phys. Chem. A* **2000**, *104*, 6566−6572.
(13) Seiler, R.; Kensy, U.; Dick, B. *Phys. Chem. Chem. Phys.* **2001**, *3*, 5373−5382.
(14) Giugni, A.; Eramo, R.; Cavalieri, S.; Pietraperzia, G.; Becucci, M.; Gellini, C.; Moroni, L.; Salvi, P. R. *Chem. Phys. Lett.* **200**, *330*, 315−324.
(15) Moroni, L.; Gellini, C.; Salvi, P. R.; Liu, C.-J.; Vogel, E. *J. Phys. Chem. A* **2002**, *106*, 6554−6562.
(16) Hay, P. J.; Shavitt, I. *J. Chem. Phys.* **1974**, *60*, 2865−2877.
(17) Matos, J. M.; Roos, B. O.; Malmqvist, P.-A. *J. Chem. Phys.* **1987**, *86*, 1458−1466.
(18) Kato, S. *J. Chem. Phys.* **1988**, *88*, 3045−3056.
(19) Palmer, M. H.; Walker, I. C. *Chem. Phys.* **1989**, *133*, 113−121.
(20) Orlandi, G.; Palmieri, P.; Tarroni, R.; Zerbetto, F.; Zgierski, M. Z. *J. Chem. Phys.* **1994**, *100*, 2458−2464.
(21) S. Zilberg, Y. H.; Shaik, S. *J. Phys. Chem.* **1995**, *99*, 16558−16565.
(22) Vogel, E.; Reel, H. *J. Am. Chem. Soc.* **1972**, *94*, 4388−4389.
(23) Vogel, E.; Vogel, A.; Kübbeler, H. K.; Sturm, W. *Angew. Chem., Int. Ed.* **1970**, *9*, 514−516.
(24) Dupuis, M.; Spangler, D.; Wendoloski, J. J. *NRCC Software Catalog*, vol.1, program n. QG01, *GAMESS*; 1980.
(25) Bianchi, R.; Casalone, G.; Simonetta, M. *Acta Crystallogr. B* **1975**, *31*, 1207−1209.
(26) Gavezzotti, A.; Mugnoli, A.; Raimondi, M.; Simonetta, M. *J. Chem. Soc., Perkin II* **1972**, pages 425−431.
(27) Nendel, M.; Houk, K. N.; Tolbert, L. M.; Vogel, E.; Jiao, H.; v. R. Schleyer, P. *J. Phys. Chem. A* **1998**, *102*, 7191−7198.
(28) Nendel, M.; Houk, K. N.; Tolbert, L. M.; Vogel, E.; Jiao, H.; v. R. Schleyer, P. *Angew. Chem., Int. Ed. Engl.* **1997**, *36*, 748−750.
(29) Julg, A.; Francois, P. *Theor. Chim. Acta* **1967**, *8*, 249−259.
(30) Dewar, M. J. S.; Dougherty, R. C. *PMO Theory in Organic Chemistry*; Plenum: New York, 1975.
(31) Moffitt, W. *J. Chem. Phys.* **1954**, *22*, 320−333.
(32) Coulson, C.; Rushbrooke, G. *Proc. Cambridge Philos. Soc.* **1940**, *36*, 193−200.
(33) Pariser, R. *J. Chem. Phys.* **1956**, *26*, 250−268.
(34) Nakano, H. *J. Chem. Phys.* **1993**, *99*, 7983−7992.
(35) Nakano, H.; Yamanishi, M.; Hirao, K. *Trends Chem. Phys.* **1997**, *6*, 167−214.
(36) Albrecht, A. C. *J. Chem. Phys.* **1961**, *34*, 1476−1484.
(37) Albrecht, A. C.; Hutley, M. C. *J. Chem. Phys.* **1971**, *55*, 4438−4443.
(38) Tang, J.; Albrecht, A. C. In *Raman Spectroscopy. Theory and Practice*; Szymansky, H. A., Ed.; Plenum: New York, 1970.
(39) Clark, R. J. H.; Dines, T. J. *Angew. Chem., Int. Ed. Engl.* **1986**, *25*, 131−158.
(40) Bonang, C. C.; Cameron, S. M. *J. Chem. Phys.* **1992**, *97*, 5377−5383.
(41) Ohta, N.; Ito, M. *Chem. Phys.* **1977**, *20*, 71−81.
(42) Gallagher, S. H.; Armstrong, R.; Clucas, W. A.; Lay, P. A.; Reed, C. A. *J. Phys. Chem. A* **1997**, *101*, 2960−2968.
(43) Bree, A. *Chem. Phys. Lett.* **1986**, *131*, 65−69.
(44) Manneback, C. *Physica* **1951**, *17*, 1001−1010.
(45) Clark, R. J. H.; Dines, T. J. *Mol. Phys.* **1981**, *42*, 193−207.
(46) Siebrand, W.; Zgierski, M. Z. *J. Phys. Chem.* **1982**, *86*, 4718−4725.
(47) Ziegler, L. D.; Hudson, B. *J. Chem. Phys.* **1981**, *74*, 982−992.